AGU PUBLICATIONS

Geophysical Research Letters

RESEARCH LETTER
10.1002/2017GL076216

Key Points:
- Repose periods are essential in resetting permeability response prior to reactivation
- Continuous sealing during hold is consistent with power law compaction
- Reactivated permeability response switches from net reduction (brief repose) to net increase (extended repose)

Supporting Information:
- Supporting Information S1
- Data Set S1
- Data Set S2

Correspondence to:
K. Im,
kxi123@psu.edu

Citation:
Im, K., Elsworth, D., & Fang, Y. (2018). The influence of preslip sealing on the permeability evolution of fractures and faults. *Geophysical Research Letters, 45*. https://doi.org/10.1002/2017GL076216

Received 20 JUL 2017
Accepted 27 DEC 2017
Accepted article online 3 JAN 2018

The influence of Preslip Sealing on the Permeability Evolution of Fractures and Faults

Kyungjae Im[1], Derek Elsworth[1], and Yi Fang[1,2]

[1]Department of Energy and Mineral Engineering, EMS Energy Institute, and G3 Center, Pennsylvania State University, University Park, PA, USA, [2]Now at Institute for Geophysics, Jackson School of Geosciences, The University of Texas Austin, Austin, TX, USA

Abstract The evolution of permeability on fractures and faults during the full earthquake cycle is shown to be sensitive to sealing during the repose phase. We explore the combined effect of static loading followed by fracture reactivation on permeability evolution via slide-hold-slide experiments. During the hold periods, permeability exhibits a slow but continuous reduction. The permeability decay is consistent with power law compaction of the aperture coupled with cubic law flow. With increasing hold periods, permeability evolves following reactivation from net reduction to net increase with the magnitude of the permeability change dependent on the hold period. This implies that the tight interlocking of asperities during interseismic repose primes the fault for permeability enhancement following reactivation. The inferred mechanism is via shear dilation with the probable involvement of unclogging. This result identifies that preslip sealing during repose is an essential component in the cyclic permeability evolution throughout the seismic cycle.

1. Introduction

The evolution of permeability on fractures and faults is known to be sensitive to changes in effective stresses. Permeability evolves as a result of both static and dynamic stress perturbations throughout the earthquake cycle (Brodsky et al., 2003; Elkhoury et al., 2006; Manga et al., 2003, 2012; Roeloffs, 1998; Rojstaczer & Wolf, 1992; Wang & Manga, 2015; Wang et al., 2016), as a result of reservoir stimulation (Mukuhira et al., 2017; Zoback et al., 2012) and potentially in the sequestration of energy wastes (Fang et al., 2017). Shear dilation contributes to increases in permeability and has been explored with analytic models (Elsworth & Goodman, 1986; Hossain et al., 2002; Liu et al., 2000) and field-scale observations (Guglielmi et al., 2015). Not surprisingly, this response exhibits some of the attributes of rate-dependent properties of fault friction (Fang et al., 2017; Ishibashi et al., 2016) as implied by rate-state characterizations of fault friction and shear dilation (Segall & Rice, 1995; Samuelson et al., 2009).

Observations have demonstrated the importance of comminution/compaction in conditioning permeability evolution (Fang et al., 2017; Faoro et al., 2009; Zhang et al., 1999), especially at the initiation of slip. However, this response may be spuriously influenced by artifacts of the initial experimental conditions (an artificial surface and fresh contacts) and do not necessarily represent a fault that has healed and sealed during its interseismic repose. Pressure solution and stress corrosion during static loading (Chen & Spiers, 2016; Gratier et al., 2014; Lehner, 1995; Polak et al., 2003; Yasuhara & Elsworth, 2008; Yasuhara et al., 2003, 2004, 2006) may tightly interlock asperities and develop local roughness on the contact surface. Shear slip on the tightly mated surface may subsequently induce sustained (long-duration) dilation via asperity dislocation. Thus, the incorporation of healing and concomitant sealing during repose may be an essential requirement to follow the correct evolution of permeability. Such sealing has been inferred both at field and laboratory scales (Elkhoury et al., 2006, 2011; Giger et al., 2007; Xue et al., 2013; Wang et al., 2016), over periods of years to hours, together with permeability enhancement at the onset of dynamic loading and slip.

In the following, we investigate the combined effect of static loading and shear deformation on fracture permeability. We measure permeability continuously during shear reactivation of fractures with intervening periods of static loading on samples of westerly granite and Green River shale.

2. Experimental Method

We explore this response through fluid-through-flow experiments in a triaxial pressure cell with independent application of confining pressure, shear stress, and pore pressure (see Figure 1a). A prismatic rock coupon in

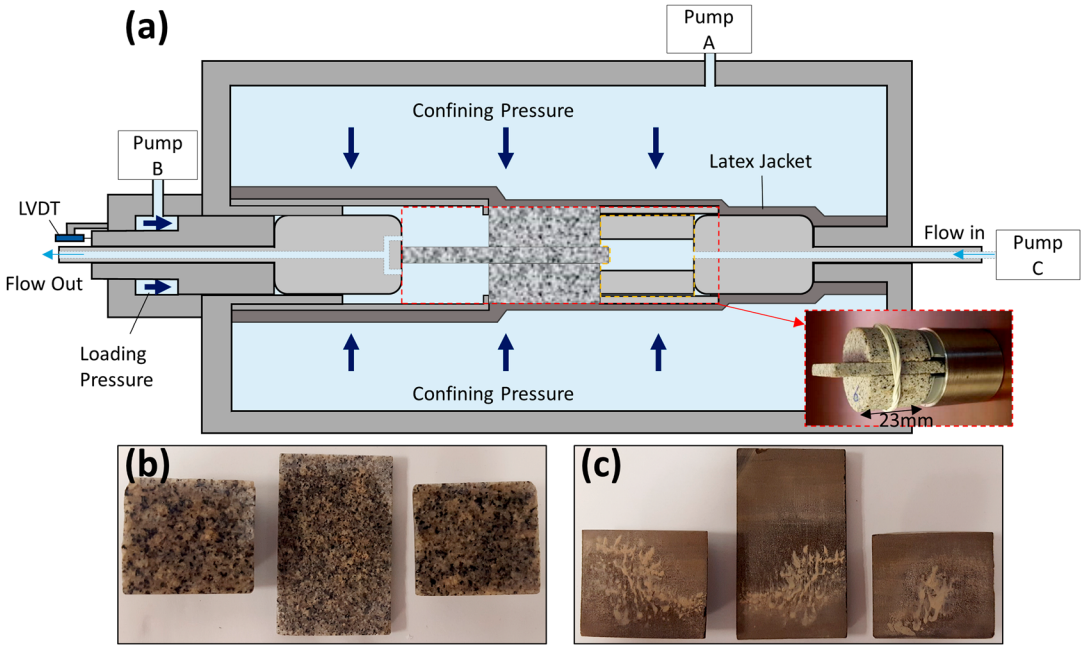

Figure 1. (a) Experimental configuration. Servo pumps control confining stress (pump A), loading pressure (pump B), and flow pressure difference (pump C). Bottom right picture in Figure 1a shows the westerly granite sample used in this experiment. (b and c) Surface conditions after experiments for westerly granite and Green River shale, respectively. Orange dashed box denotes inlet chamber that affects apparent permeability (see text).

double direct shear configuration (35 mm × 24 mm × 3 mm) is sandwiched between half-cylindrical cores within a latex jacket. This experimental configuration enables accurate measurement of friction by minimizing the impact of jacket/membrane restraint. Experimental variables include surface roughness (ground with #150 grit (rougher) and #600 grit (smoother) aluminum powder) and mineralogy (westerly granite (WG, tectosilicate >90%) and Green River shale (GRS, tectosilicate ~46%, carbonate ~52%, and phyllosilicate ~2%, Fang et al., 2017)).

The permeating fluid is de-ionized and de-aired water supplied from an upstream pump and flowing along the two parallel fractures (Figure 1). The confining/normal stress, inlet/outlet pressure difference, and shear loading rate are independently controlled by three servo-controlled pumps. Pump A controls confining pressure that is retained constant at 3 MPa. Loading rate and induced shear stress are controlled/measured by pump B with prescribed flow rate. Displacement rates are confirmed through the volume rates of pump B together with measurements of a linear variable differential transducer (LVDT) connected to the loading piston. Resulting flow rates are recorded continuously during multiple slide and hold experiments by pump C, with longitudinal fluid pressure differences limited to 30 kPa to 200 kPa (~7% of total stress) for all experiments.

Permeability (k) is calculated from Darcy's law as

$$k = \frac{\mu L}{A}\frac{Q}{\Delta P}, \tag{1}$$

where μ is fluid viscosity (8.9×10^{-4} Pa s), L is flow path length (23 mm), A is cross-sectional area of the sample perpendicular to the flow path (4.71×10^{-4} m^2), Q is flow rate, and ΔP is the pressure difference across the sample. In this configuration, flow rate Q is directly proportional to the permeability evolution as L, A, and ΔP are constant.

This novel experimental configuration enables concurrent and continuous measurement of both permeability and friction throughout static and dynamic motion—but entrains a minor artifact that appears in the experimental results. When the upstream reservoir volume (orange dashed line in Figure 1a) is reduced by shear slip, an identical volume is also reduced in the flow rate of pump C to maintain constant pressure. Due to this effect, a false step reduction of "apparent" permeability appears at the activation of shear slip (and step increase at hold). This effect is generally trivial but can be observable when the flow rate is also small. Apparently, these effects are inconsequential for the experiments reported here.

We conduct slide-hold-slide (SHS) experiments in modes involving (i) five single long holds and also as (ii) three repeating slide-hold-slides (see Table S1 in the supporting information for experiment list). All experiments initiate with the application of confining pressure (3 MPa) followed by the pressure saturation of the sample until flow stabilizes. The samples are sheared-in at a constant velocity 10 μm/s. The single long hold mode is designed to investigate sealing behavior during the hold period; therefore, only one long hold is applied after initial shear reaches a preset distance (3~7 mm). For the repeating slide-hold-slide mode, initial shear displacements are set to 2 mm followed by hold periods punctuated by reactivations (slide-hold-slide). The hold periods, representing interseismic repose, are systematically increased for the SHS experiment between intervening shear phases. Successive incremental hold periods are of 10 s, 30 s, 100 s, 300 s, 1,000 s, 3,000 s, and 10,000 s with intervening reactivations of 1 mm at a velocity of 10 μm/s. Exceptions to these conditions are where the pump was already empty before the final 10,000 s hold (rougher granite) and where an extra hold (5,000 s) was applied after the final slip period (smoother granite).

3. Results

3.1. Sealing

Figure 2 presents five long hold mode experiment results. All specimens exhibit continuous decay without evidences of stabilization within the experimental duration. The curves initially appear to follows linear trend in log-log plot. However, after a few hours, the curves deviate from the linear trend toward faster decay.

Interestingly, these results are plausibly described as power law compaction (in time) (e.g., Gratier et al., 2014), coupled with permeability evaluated from the cubic law. Assuming that compaction follows a power law, time-dependent aperture reduction (Δb) can be described by a power exponent n as

$$\Delta b = \alpha t^n, \tag{2}$$

where t is time and α is the compaction displacement at $t = 1$. Permeability k may be defined relative to compaction in aperture (Δb) (Ouyang & Elsworth, 1993; Witherspoon et al., 1980) as

$$k = k_0 \left(1 - \frac{\Delta b}{b_0}\right)^3, \tag{3}$$

where k_0 and b_0 denote an initial permeability and aperture, respectively. Substituting equation (2) into (3) yields

$$k = k_0 \left(1 - \frac{\alpha}{b_0} t^n\right)^3. \tag{4}$$

The resulting model fits to experimental results are presented in Figure 2 (black dotted lines) using equation (4) with parameters (k_0, α/b_0, and n) presented in Figure 2a. The plots show that the model adequately represents permeability reduction behaviors with the power exponents n = 0.3–0.4.

We estimate the magnitude of compaction during the hold by converting the permeability to equivalent hydraulic aperture (h) of each fracture with the cubic law relation (Witherspoon et al., 1980):

$$h = \left(\frac{Q}{2}\frac{L}{\Delta P}\frac{12\mu}{w}\right)^{\frac{1}{3}}, \tag{5}$$

where the notations are identical to equation (1) with w denoting fracture width (21 mm). Note that Q is halved since our experimental configuration embeds two fractures. Figure 2 shows that the longest hold experiment (TKH9) resulted in an ~85% permeability decline during ~22 h of hold (from $k = 1.4 \times 10^{-15}$ m^2 to 2.1×10^{-16} m^2). From equations (5) and (1), this yields 2.6 μm of equivalent hydraulic aperture change (from 5.7 μm to 3.1 μm), illustrating the extreme sensitivity of permeability to aperture change.

The shear permeability responses of TKH9 are zoomed-in in the upper right portion of Figure 2b, showing a clear conversion from shear-induced permeability destruction to enhancement. The left inset shows permeability response with the initial 3 mm slip, and the right inset shows permeability response with 1 mm slip after ~22 h of hold. A trend of permeability decrease for the initial 3 mm of slip (red background) continues until the hold phase begins (shear/hold boundary shows the artifacts discussed in section 2). This declining

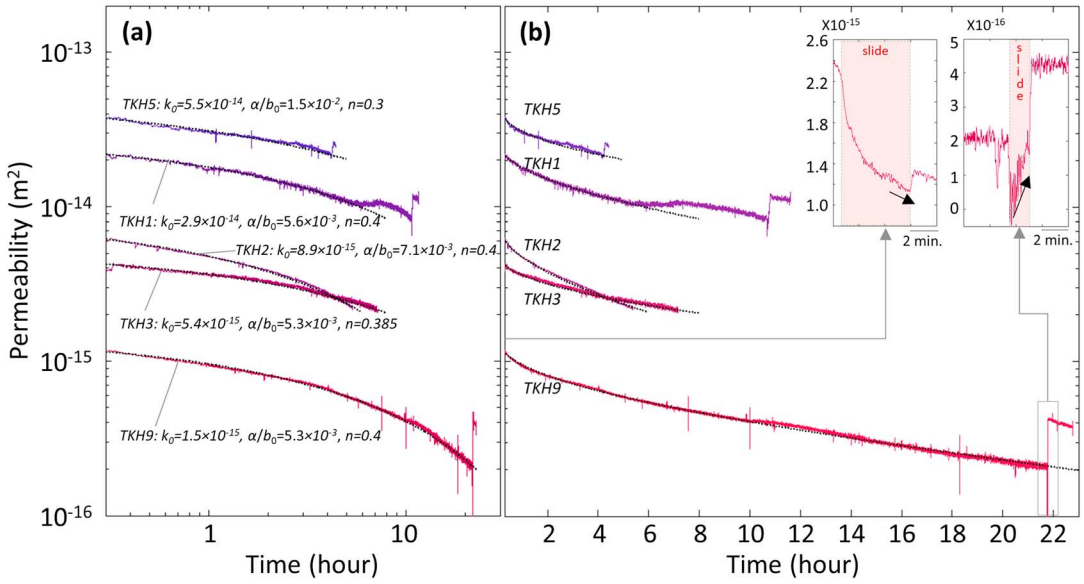

Figure 2. Permeability decay with time. Five single long hold experiments conducted with westerly granite with different roughnesses shown on (a) log-log and (b) log linear scales. Time zero is set when normal stress reaches 3 MPa. Black dotted lines, overlapping on the experimental result, are model fits using power law compaction and cubic law for flow (see text for method) with fitting parameters listed in Figure 2a. Insets in Figure 2b show permeability response of TKH9 for an initial 3 mm slip (left) and further 1 mm slip after ~21 h of hold (right). The temporal permeability reductions during slip in the insets are artifacts due to the volume of sample intrusion into the inlet chamber. Step increase of permeability of TKH1 and TKH5 result from shear slip. We do not have a clear explanation for the gradual permeability enhancement of TKH1 shown at time ~6–8 h but find that it occurs with gradual shear stress reduction (not shown here).

trend reverses into significant enhancement after 22 h of hold, resulting in a roughly 100% increase in permeability during the subsequent 1 mm of slip.

3.2. Permeability Response to Repeating Slide-Hold-Slide Motion

Figure 3 shows shear stress and flow rate responses during slide-hold-slide experiments extending for ~6 h. Periods of slip and intervening hold are denoted by the top bar of Figure 3a with experiments exhibiting typical rate-state frictional response. Applied shear stresses decline during the hold then increase sharply to a peak during reactivation before stabilizing, following rate and state friction (Marone, 1998). The magnitude of the peak stress increases with the increased duration of the prior hold period, representing time-dependent frictional healing.

Figure 3b presents permeability evolution for all cases. It shows that the permeability is larger for rougher sample (#150 grit) than smoother sample (#600 grit) and harder sample (WG) than weaker sample (GRS). This observation naturally resulted from larger aperture (or pore throat) with rougher surface and may reflect significant pore throat destruction during application of normal stress on weak rock surface (GRS).

Early time response in Figure 3b shows the decline rate in permeability is anomalously large during the initial shearing-in period for all samples. A zoomed-in view of the initial decline (Figure 3c) shows that this initial permeability reduction immediately follows the initiation of shear slip (i.e., driven by slip) and the decline rate is significantly reduced after a few millimeters of slip. Normalized permeability reduction during this initial period is greater for weaker rock (GRS) than for stronger/harder rock (WG) and with smoother rather than rougher surfaces (see Figure 2b, early time). These observations, together with the observed production of comminution products (GRS) during the experiment (Figure 1c), suggest that the initial strong permeability reduction is mainly as a result of comminution/compaction and wear products from the fracture surfaces. This is especially dominant on fresh artificial samples that may not necessarily represent natural faults and fractures.

Further reactivations following incremented durations of static loading (hold periods) show significant permeability enhancements. Figure 3d highlights the permeability responses of the later stage reactivations and interslip holds of smoother WG (period identified by rectangles in Figure 2b). This plot clearly identifies a

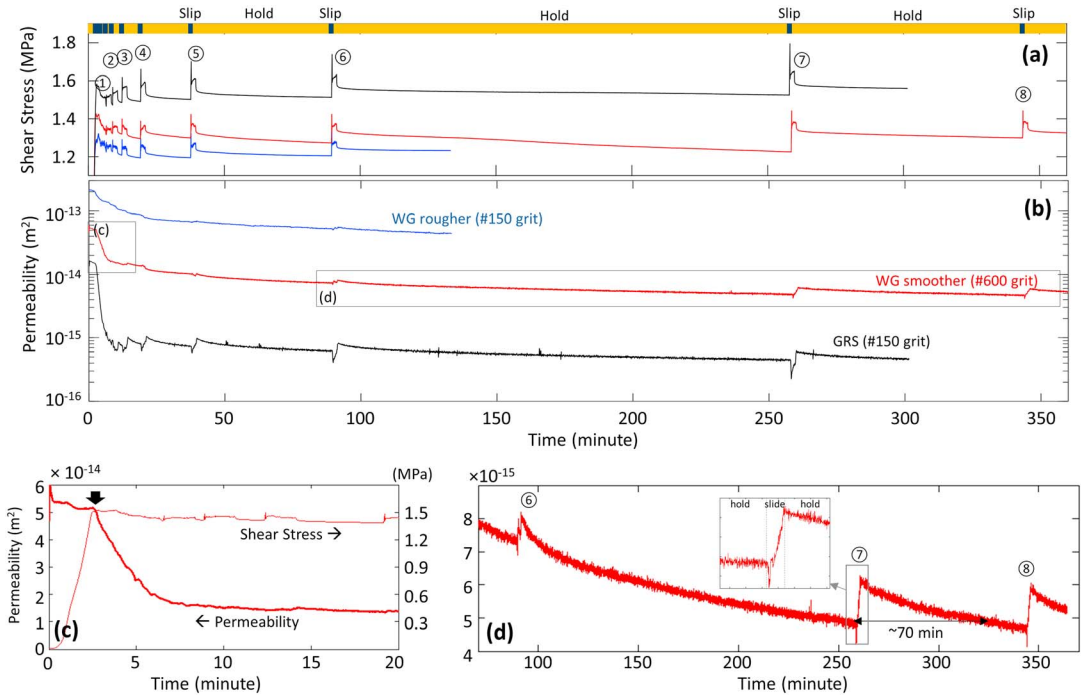

Figure 3. Friction and permeability response during slide and hold experiments. Each color denotes rock and surface roughness: blue: westerly granite rougher sample (#150 grit), red: WG smoother (#600 grit), and black: Green River shale (#150 grit). (a and b) Shear stress and permeability response during the overall experiment, respectively. Slip and hold periods are denoted on the top of Figure 3a by blue and orange bars, respectively. Circled numbers denote event numbers used in text. (c and d) Zoomed-in views of the box insert in Figure 3b. The downward arrow in Figure 3c represents the initiation of shear slip. Single responses to sliding are highlighted in the small box in Figure 3d. Detailed view of WG rougher and GRS cases are provided in the supporting information (Figure S2).

cyclic repetition of permeability destruction (interslip sealing) and then creation (shear permeability enhancement). For instance, permeability continuously decreases during the 10,000 s hold between slips ⑥ and ⑦ yielding a permeability reduction of ~37.5% (from ~8 × 10^{-15} m^2 to ~5 × 10^{-15} m^2). In the following slip ⑦, permeability increases by ~25% within 1 mm of shear deformation (<5% of contact length) before permeability again decreases at the conclusion of the slip phase. It takes ~70 min to recover to the original permeability prior to the slip ⑦.

Zoomed-in views in Figure 3d show that the permeability enhancement behaviors are gradual as observed in the inset of Figure 2b. Permeability continues to increase over 1 mm slips. This length scale (>1 mm) is far larger than critical displacements for the evolution of friction observed in these experiments (10–20 μm, see Figure S1). The permeability evolution does not show an abrupt destruction at the beginning of the hold phase—conversely, it exhibits a sustained and slow decline. These behaviors are similarly observed in the two other cases (see Figure S2).

3.3. Permeability Enhancement and Hold Duration

SHS experiments (Figure 3) show initial reactivation results in a strong reduction in permeability, but this switches to significant enhancement after an extended period of healing. These are exhibited in Figures 4a (rougher WG), 4b (smoother WG), and 4c (GRS) with response typified in Figure 4a (rougher WG). This represents sequential changes in permeability response that show significant net initial declines (①, ②, ③, and ④), transitioning to a net increases (⑤) that becomes more significant (⑥).

Permeability enhancements resulting from various hold durations are shown in Figures 4d (absolute increase Δk) and 4e (normalized increase, $\Delta k/k_0$). The larger ultimate enhancements scale increasing roughness and hardness, implicating the essential role of shear dilation. The magnitude of absolute permeability enhancement (Figure 4d) is largest with stiffer/stronger/rougher granite and smallest with weaker/smoother shale. Conversely, the magnitude of normalized permeability enhancement (Figure 4e) is largest with shale and smallest with rougher granite. This behavior is substantially implied by the cubic law (equation (3)).

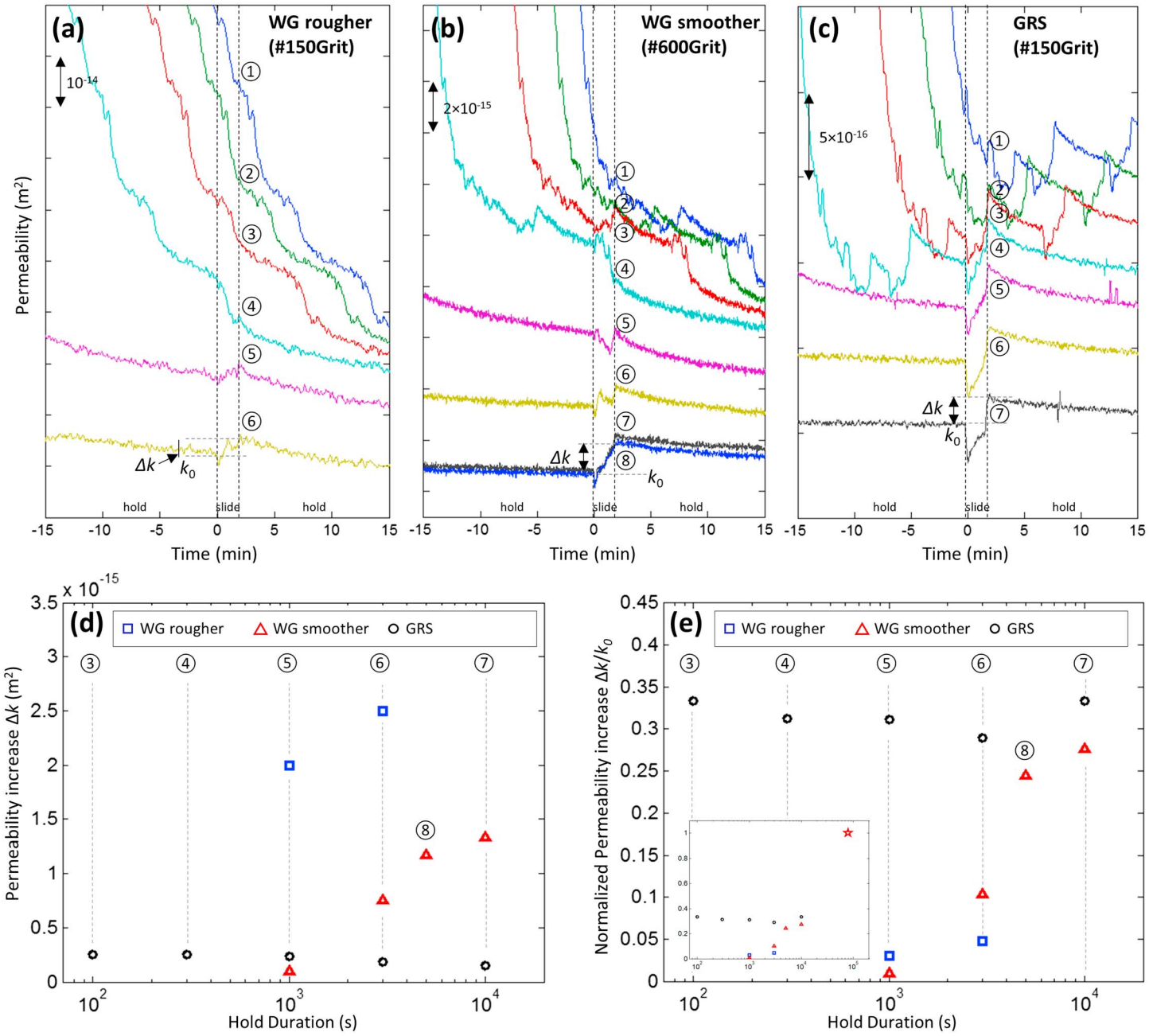

Figure 4. Sequence of permeability evolution of (a) WG rougher, (b) WG smoother, and (c) GRS. All slip events are aligned with reactivation ($t = 0$ s). (d) Absolute and (e) normalized permeability enhancement versus hold duration. Definition of permeability enhancement Δk and initial permeability k_0 is shown in Figures 4a–4c. Circled numbers correspond to event number in Figure 2. The colors and symbols denotes rock and roughness: WG rough (blue square), WG smooth (red triangle), and GRS (black circle). Inset in Figure 4e includes TKH9 results (Figure 3c insets) denoted by a red star.

Although shear aperture increase ($-\Delta b$) is largest with a rougher/hard surface, normalized permeability enhancement can be smallest due to the large initial aperture (b_0).

The permeability enhancement of westerly granite significantly increases with an extended duration of healing in both absolute (Figure 4d) and relative magnitudes (Figure 4e), implying, especially for hard rock, that the magnitude of shear permeability enhancement is dependent on the preslip healing/sealing. For the case of the smoother granite (Figure 4d), no shear permeability enhancement appears after only short healings, ~1% of enhancement induced after 1,000 s of healing, and ~27% after 10,000 s. Permeability enhancement appears approximately log linear with preslip hold duration. The inset in Figure 4e shows

that the largest normalized permeability enhancement is achieved with the longest hold time (TKH9, Figure 3b insets).

4. Discussion

4.1. Mechanism for Permeability Evolution

Shear slip may destroy the permeability by comminution/compaction or conversely create it by breaching the mated contact surface. These two contrasting behaviors may be controlled by the fidelity of the interlocking surfaces, that is, sealing. For instance, if the two surface asperities are strongly mated via long-duration healing and sealing, shear slip may result in permeability enhancement. Conversely, if the surfaces are artificially prepared, fresh, and unsealed, shear slip may collapse bridging contacts and result in strong permeability reduction.

Strong permeability reduction is observed upon initial shear reactivation. Normalized permeability reduction is larger for weaker rocks (GRS) and smoother surface textures (#600 grit). The presence of observable wear product with GRS (Figure 1c) suggests that initial strong permeability reduction is driven by shear comminution effects. These observations, and those of prior studies (e.g., Faoro et al., 2009; Ishibashi et al., 2016; Tanikawa et al., 2010; Fang et al., 2017; Zhang et al., 1999), demonstrate that this strong permeability reduction is especially significant during the initial shear-in process on fresh, laboratory-prepared surfaces.

Conversely, sealing is always active even when the influence of comminution becomes trivial. In our experiments, permeability decay can be plausibly described by power law compaction coupled with the cubic law. The slow but continuous permeability decay may imply that mechanochemical effects governs the sealing behavior observed in these experiments. Interestingly, despite the difference in contact geometry, power law compaction is analogously observed with solution-driven transport around a rigid indenter and exhibits a similar range of power exponents (0.3–0.4) (Gratier et al., 2014). Since the dissolution rate of quartz is known to be insignificant at room temperature (Dove & Crerar, 1990), stress corrosion (Polak et al., 2003; Yasuhara & Elsworth, 2008) may primarily drive this slow compaction process. This may be aided by pressure solution of fine wear products that may be bridged in between the contacts, by mineral precipitation on the pore space, and by flux driven wear product clogging.

Dilation is inferred by the absolute magnitude of permeability creation being largest for harder (granite) and rougher surfaces. The process of shear dilation and frictional properties (rate and state) imply a rate dependency of permeability consistent with strength evolution on faults (Fang et al., 2017; Ishibashi et al., 2016). The rate dependency of fracture aperture (porosity) model is suggested by anticipated dilation rates (Samuelson et al., 2009; Segall & Rice, 1995):

$$\phi_{ss} = \phi_0 + \varepsilon \ln\left(\frac{v}{v_0}\right), \tag{6}$$

where ϕ_{ss} is steady state porosity, ϕ_0 is reference porosity, ε is dilatancy coefficient, v is velocity, and v_0 is reference velocity. If coefficients ϕ_0 and ε are constants, then, absent the production of wear products, permeability enhancement via constant shear velocity is only dependent on the magnitude of preslip sealing. Where permeability scales as $k/k_0 = (1 + \Delta\phi/\phi_0)^3$ (equation (3)), a significant shear permeability enhancement will result on a strongly sealed fracture. Dilation is inferred by the observation that the absolute magnitude of permeability creation is largest for the harder (granite) and rougher surfaces.

We observe a gradual enhancement in shear permeability. Permeability enhancement occurs over a longer distance ($>$1 mm) than the critical frictional slip distance ($D_c \sim$ 10–20 μm, Figure S1). And the permeability reduction is also slow and gradual as observed by natural permeability response to earthquakes (Elkhoury et al., 2006; Xue et al., 2013). Such a gradual evolution has been observed in some existing studies on shear dilation (Neimeijer et al., 2008, 2010; Chen et al., 2015) and permeability evolution (Fang et al., 2017; Ishibashi et al., 2016) including models of granular friction and permeability (Wang et al., 2017).

The presence of wear products in GRS sample (Figure 1c) suggests that the permeability enhancement may be associated with flux-driven unclogging of the fracture (Candela et al., 2014, 2015; Elkhoury et al., 2011). Although our experiments are conducted with constant pressure, pore throat expansion due to shear dilation may trigger the release of trapped wear products and unclog any colloidal seal. We mimic prior oscillatory

pressure pulse experiments with WG (see Figure S3) and confirm that significant permeability enhancement may result. Moreover, these experiments confirm that permeability can be further enhanced when shear slip (induced seismicity) is triggered by the pressure pulse. The difference in the amount of visible wear product between WG and GRS (Figures 1b and 1c) suggests that the observed difference in permeability response to shear (Figures 4d and 4e) can also be influenced by the unclogging process.

4.2. Implication to Natural Systems

These experiments suggest that commonly observed coseismic and postseismic permeability enhancements may also be contributed to by shear slip. Our experiments suggest that preslip sealing is an essential process to allow shear permeability enhancement. Indeed, the sealing process is inferred by field observations that show permeability reduction (Elkhoury et al., 2006; Xue et al., 2013) and hydraulic decoupling of aquifers (Wang et al., 2016) following coseismic reactivation. A long duration of interseismic sealing can reset the fault permeability, priming it for another cycle of coseismic permeability enhancement followed by its slow destruction.

These experimental results recall the potential of permeability characterizations as potentially sensitive earthquake precursors (e.g., Roeloffs, 1998, 2006). Seismic events may transition through an aseismic nucleation phase until the slip patch reaches a critical size (Dieterich, 1992; Rice, 1993), which may generate detectable signals. Recently, active measurements of reduction in seismic velocity have been linked to preslip frictional weakening (Scuderi et al., 2016). Similarly, permeability enhancement during nucleation, which is potentially driven by the same fundamental mechanism to frictional weakening (Samuelson et al., 2009; Segall & Rice, 1995), could be viewed as a sensitive precursor. This would require a sufficiently long duration of interseismic healing together with a preslip distance large enough and an observation wellbore sufficiently hydraulically well connected to the preslip fault plane. In the experimental results, we show that even 1 mm of slow-fault reactivation can result in a significant permeability enhancement.

Fracture permeability has been observed to be enhanced by transient stresses induced by distant earthquakes (Brodsky et al., 2003; Manga et al., 2012). The behavior has been attributed to transient-flux-driven (sloshing) unclogging of colloidal seals (Brodsky et al., 2003; Candela et al., 2014, 2015; Elkhoury et al., 2011). Our experiments suggest that remotely triggered seismicity (and therefore fault shear) (e.g., Hill et al., 1993; Van der Elst et al., 2013) should also be considered in explaining permeability enhancement. Transiting seismic waves from distant earthquakes will selectively reactivate the local fault patches that are near-critically stressed. The model can explain why the permeability response can be observed only in particular wellbores (e.g., Brodsky et al., 2003; Wang et al., 2016) since the response will be only significant for wellbores that are hydraulically connected to any reactivated fault patches. Further, earthquake-induced hydraulic connection between vertically stacked aquifers, observed by Wang et al. (2016), can be described by simply assuming that the reactivated fault transects the boundary between the two aquifers.

5. Conclusion

Our experiments demonstrate a cycle of the creation then destruction of permeability during laboratory slide-hold-slide experiments, which substantially reproduce natural observations (Elkhoury et al., 2006). We observe that both comminution and dilation can be driven by shear slip. The comminution effect is mostly dominant during initial shear-in on artificial fresh surfaces and for short healing/sealing periods—which may not be broadly representative of natural systems. Conversely, the effects of dilation become increasingly significant with the increased duration of healing—conditions much more representative of natural condition on faults subject to interseismic repose. During experimentally imposed periods of hold the permeability continuously declines, described by power law compaction and cubic law flow. Upon reactivation, the magnitude of permeability increase scales with an increase in repose period. Indeed, applying a substantial prereactivation repose period is essential to follow the correct path of permeability evolution present through the seismic cycle.

Acknowledgments
All experimental data are available as supporting information. This work is a partial result of support from the U.S. Department of Energy (DOE) under projects DE-FE0023354. This support is gratefully acknowledged.

References

Brodsky, E. E., Roeloffs, E., Woodcock, D., Gall, I., & Manga, M. (2003). A mechanism for sustained groundwater pressure changes induced by distant earthquakes: *Journal of Geophysical Research*, *108*(B8), 2390. https://doi.org/10.1029/2002JB002321

Candela, T., Brodsky, E. E., Marone, C., & Elsworth, D. (2014). Laboratory evidence for particle mobilization as a mechanism for permeability enhancement via dynamic stressing. *Earth and Planetary Science Letters*, *392*, 279–291. https://doi.org/10.1016/j.epsl.2014.02.025

Candela, T., Brodsky, E. E., Marone, C., & Elsworth, D. (2015). Flow rate dictates permeability enhancement during fluid pressure oscillations in laboratory experiments. *Journal of Geophysical Research: Solid Earth*, *120*, 2037–2055. https://doi.org/10.1002/2014JB011511

Chen, J., & Spiers, C. (2016). Rate and state frictional and healing behavior of carbonate fault gouge explained using microphysical model. *Journal of Geophysical Research: Solid Earth*, *121*, 8642–8665. https://doi.org/10.1002/2016JB013470

Chen, J., Verberne, B. A., & Spiers, C. J. (2015). Interseismic re-strengthening and stabilization of carbonate faults by "non-Dieterich " healing under hydrothermal conditions. *Earth and Planetary Science Letters*, *423*, 1–12. https://doi.org/10.1016/j.epsl.2015.03.044

Dieterich, J. H. (1992). Earthquake nucleation on faults with rate- and state-dependent strength. *Tectonophysics*, *211*(1-4), 115–134. https://doi.org/10.1016/0040-1951(92)90055-B

Dove, P. M., & Crerar, D. A. (1990). Kinetics of quartz dissolution in electrolyte solutions using a hydrothermal mixed flow reactor. *Geochimica et Cosmochimica Acta*, *54*(4), 955–969. https://doi.org/10.1016/0016-7037(90)90431-J

Elkhoury, J. E., Brodsky, E. E., & Agnew, D. C. (2006). Seismic waves increase permeability. *Nature*, *441*(7097), 1135–1138. https://doi.org/10.1038/nature04798

Elkhoury, J. E., Niemeijer, A., Brodsky, E. E., & Marone, C. (2011). Laboratory observations of permeability enhancement by fluid pressure oscillation of in situ fractured rock. *Journal of Geophysical Research*, *116*, B02311. https://doi.org/10.1029/2010JB007759

Elsworth, D., & Goodman, R. E. (1986). Characterization of rock fissure hydraulic conductivity using idealized wall roughness profiles. *International Journal of Rock Mechanics and Mining Science & Geomechanics*, *23*, 233–243.

Fang, Y., Elsworth, D., Wang, C., Ishibashi, T., & Fitts, J. P. (2017). Frictional stability-permeability relationships for fractures in shales. *Journal of Geophysical Research: Solid Earth*, *122*, 1760–1776. https://doi.org/10.1002/2016JB013435

Faoro, I., Niemeijer, A., Marone, C., & Elsworth, D. (2009). Influence of shear and deviatoric stress on the evolution of permeability in fractured rock. *Journal of Geophysical Research*, *114*, B01201. https://doi.org/10.1029/2007JB005372

Giger, S. B., Tenthorey, E., Cox, S. F., & Gerald, J. D. F. (2007). Permeability evolution in quartz fault gouges under hydrothermal conditions. *Journal of Geophysical Research*, *112*, B07202. https://doi.org/10.1029/2006JB004828

Gratier, J. P., Renard, F., & Vial, B. (2014). Postseismic pressure solution creep: Evidence and time-dependent change from dynamic indenting experiments. *Journal of Geophysical Research: Solid Earth*, *119*, 2764–2779. https://doi.org/10.1002/2013JB010768

Guglielmi, Y., Cappa, F., Avouac, J., Henry, P., & Elsworth, D. (2015). Seismicity triggered by fluid injection-induced aseismic slip. *Science*, *348*(6240), 1224–1226. https://doi.org/10.1126/science.aab0476

Hill, D. P., Reasenberg, P. A., Michael, A., Arabaz, W. J., Beroza, G., Brumbaugh, D., … Zollweg, J. (1993). Seismiciy remotely triggered by the magnitude 7.3 Landers, California, earthquake. *Science*, *260*, 1617–1623.

Hossain, M. M., Rahman, M. K., & Rahman, S. S. (2002). A shear dilation stimulation model for production enhancement from naturally fractured reservoirs. *SPE Journal*, *7*(2), 183–195. https://doi.org/10.2118/78355-PA

Ishibashi, T., Asanuma, H., Fang, Y., Wang, C., & Elsworth, D. (2016). Exploring the link between permeability and strength evolution during fracture shearing: Proceedings: 50th US Rock Mechanics/ Geomechanics Symposium Houston, Texas,.

Lehner, F. (1995). A model for intergranular pressure solution in open systems. *Tectonophysics*, *245*(3-4), 153–170. https://doi.org/10.1016/0040-1951(94)00232-X

Liu, J., Elsworth, D., Brady, B. H., & Muhlhaus, H. B. (2000). Strain-dependent fluid flow defined through rock mass classification schemes. *Rock Mechanics and Rock Engineering*, *33*(2), 75–92. https://doi.org/10.1007/s006030050036

Manga, M., Beresnev, I., Brodsky, E. E., Elkhoury, J. E., Elsworth, D., Ingebritsen, S. E., … Wang, C. (2012). Changes in permeability caused by transient stresses: Field observations, experiments and mechanisms. *Reviews of Geophysics*, *50*, RG2004. https://doi.org/10.1029/2011RG000382

Manga, M., Brodsky, E. E., & Boone, M. (2003). Response of streamflow to multiple earthquakes. *Geophysical Research Letters*, *30*(5), 1214. https://doi.org/10.1029/2002GL016618

Marone, C. (1998). Laboratory-derived friction laws and their application to seismic faulting. *Annual Review of Earth and Planetary Sciences*, *26*(1), 643–696. https://doi.org/10.1146/annurev.earth.26.1.643

Mukuhira, Y., Moriya, H., Ito, T., Asanuma, H., & Haring, M. (2017). Pore pressure migration during hydraulic stimulation due to permeability enhancement by low-pressure subcritical fracture slip. *Geophysical Research Letters*, *44*, 3109–3118. https://doi.org/10.1002/2017GL072809

Niemeijer, A., Marone, C., & Elsworth, D. (2008). Healing of simulated fault gouges aided by pressure solution: Results from rock analogue experiments. *Journal of Geophysical Research*, *113*, B04204. https://doi.org/10.1029/2007JB005376

Niemeijer, A., Marone, C., & Elsworth, D. (2010). Frictional strength and strain weakening in simulated fault gouge: Competition between geometrical weakening and chemical strengthening. *Journal of Geophysical Research*, *115*, B10207. https://doi.org/10.1029/2009JB000838

Ouyang, Z., & Elsworth, D. (1993). Evaluation of groundwater flow into mined panels. *International Journal of Rock Mechanics and Mining Science & Geomechanics*, 71–79.

Polak, A., Elsworth, D., Yasuhara, H., Grader, A. S., & Halleck, P. M. (2003). Permeability reduction of a natural fracture under net dissolution by hydrothermal fluids. *Geophysical Research Letters*, *30*(20), 2020. https://doi.org/10.1029/2003GL017575

Rice, J. R. (1993). Spatio-temporal complexity of slip on a fault rate- dependent friction. *Journal of Geophysical Research*, *98*(B6), 9885–9907. https://doi.org/10.1029/93JB00191

Roeloffs, E. A. (1998). Persistent water level changes in a well near Parkfield, California, due to local and distant earthquakes. *Journal of Geophysical Research*, *103*(B1), 869–889. https://doi.org/10.1029/97JB02335

Roeloffs, E. A. (2006). Evidence for aseismic deformation rate changes prior to earthquakes. *Annual Review of Earth and Planetary Sciences*, *34*(1), 591–627. https://doi.org/10.1146/annurev.earth.34.031405.124947

Rojstaczer, S., & Wolf, S. (1992). Permeability changes associated with large earthquakes: An example from Loma Prieta, California. *Geology*, *20*(3), 211–214. https://doi.org/10.1130/0091-7613(1992)020<0211:PCAWLE>2.3.CO;2

Samuelson, J., Elsworth, D., & Marone, C. (2009). Shear-induced dilatancy of fluid-saturated faults: Experiment and theory. *Journal of Geophysical Research*, *114*, B12404. https://doi.org/10.1029/2008JB006273

Scuderi, M. M., Marone, C., Tinti, E., Di Stefano, G., & Collettini, C. (2016). Precursory changes in seismic velocity for the spectrum of earthquake failure modes. *Nature Geoscience*, *9*(9), 695–700. https://doi.org/10.1038/NGEO2775

Segall, P., & Rice, J. R. (1995). Dilatancy, compaction, and slip instability of a fluid-infiltrated fault. *Journal of Geophysical Research*, *100*, 155–171.

Tanikawa, W., Sakaguchi, M., Tadai, O., & Hirose, T. (2010). Influence of fault slip rate on shear-induced permeability. *Journal of Geophysical Research*, *115*, B07412. https://doi.org/10.1029/2009JB007013

Van der Elst, N., Savage, H., Keranen, K., & Abers, G. (2013). Enhanced remote earthquake triggering at fluid-injection sites in the Midwestern United States. *Science*, 341.

Wang, C., Elsworth, D., & Fang, Y. (2017). Influence of weakening minerals on ensemble strength and slip stability of faults. *Journal of Geophysical Research: Solid Earth*, *122*, 7090–7110. https://doi.org/10.1002/2016JB013687

Wang, C., & Manga, M. (2015). New streams and springs after the 2014 M_w6.0 South Napa earthquake. *Nature Communications*, *6*, 1–6. https://doi.org/10.1038/ncomms8597

Wang, C.-Y., Liao, X., Wang, L.-P., Wang, C.-H., & Manga, M. (2016). Large earthquakes create vertical permeability by breaching aquitards. *Water Resources Research*, *340*, 5923–5937. https://doi.org/10.1002/2016WR018893

Witherspoon, P., Wang, J., Iwai, K., & Gale, J. (1980). Validity of cubic law for fluid flow in a deformable rock fracture. *Water Resources Research*, *16*, 1016–1024.

Xue, L., Li, H.-B., Brodsky, E. E., Xu, Z.-Q., Kano, Y., Wang, H., … Huang, Y. (2013). Continuous permeability measurements record healing inside the Wenchuan earthquake fault zone. *Science*, *340*(6140), 1555–1559. https://doi.org/10.1126/science.1237237

Yasuhara, H., Elsworth, D., & Polak, A. (2004). Evolution of permeability in a natural fracture: Significant role of pressure solution. *Journal of Geophysical Research*, *109*, B03204. https://doi.org/10.1029/2003JB002663

Yasuhara, H., & Elsworth, D. (2008). Compaction of a rock fracture moderated by competing roles of stress corrosion and pressure solution. *Pure and Applied Geophysics*, *165*(7), 1289–1306. https://doi.org/10.1007/s00024-008-0356-2

Yasuhara, H., Elsworth, D., & Polak, A. (2003). A mechanistic model for compaction of granular aggregates moderated by pressure solution: *Journal of Geophysical Research*, *108*(B11), 2530. https://doi.org/10.1029/2003JB002536

Yasuhara, H., Polak, A., Mitani, Y., Grader, A. S., Halleck, P. M., & Elsworth, D. (2006). Evolution of fracture permeability through fluid-rock reaction under hydrothermal conditions. *Earth and Planetary Science Letters*, *244*(1-2), 186–200. https://doi.org/10.1016/j.epsl.2006.01.046

Zhang, S., Tullis, T. E., & Scruggs, V. J. (1999). Permeability anisotropy and pressure dependency of permeability in experimentally sheared gouge materials. *Journal of Structural Geology*, *21*(7), 795–806. https://doi.org/10.1016/S0191-8141(99)00080-2

Zoback, M. D., Kohli, A., Das, I., & McClure, M. (2012). The importance of slow slip on faults during hydraulic fracturing stimulation of shale gas reservoirs. SPE Americas Unconventional Resources Conference, 5–7 June, SPE-155476-MS. Pittsburgh, PA: Society of Petroleum Engineers. https://doi.org/10.2118/155476-MS